Motility-Induced Phase Separation Mediated by Bacterial Quorum Sensing

Wesley J. M. Ridgway,[1,*] Mohit P. Dalwadi,[2,3,†] Philip Pearce,[2,3,‡] and S. Jonathan Chapman[1,§]

[1] *Mathematical Institute, University of Oxford, Oxford, OX2 6GG, UK*
[2] *Department of Mathematics, University College London, London, WC1H 0AY, UK*
[3] *Institute for the Physics of Living Systems, University College London, London, UK*

(Dated: April 1, 2023)

Abstract. We study motility-induced phase separation (MIPS) in living active matter, in which cells interact through chemical signalling, or quorum sensing. In contrast to previous theories of MIPS, our multiscale continuum model accounts explicitly for genetic regulation of signal production and motility. Through analysis and simulations, we derive a new criterion for the onset of MIPS that depends on features of the genetic network. Furthermore, we identify and characterise a new type of oscillatory MIPS that occurs when gene regulation inside cells promotes motility in higher signal concentrations.

INTRODUCTION

Chemical signals control cell motility to regulate self-organised patterning in living systems, from tissue morphogenesis and wound healing to cancer [1]. In bacterial populations, chemical signalling, or quorum sensing (QS), drives self-organisation by promoting population-level behaviours such as biofilm formation and swarming motility [2, 3]. Bacterial QS systems have been engineered to connect directly to genes controlling motility in synthetic genetic networks, enabling the generation of tunable patterns *in vitro* [4, 5]. However, we lack fundamental understanding of how cell-level features, such as gene-regulatory networks, determine emergent population-level pattern formation in living active matter.

Minimal physical models of active and living matter typically consist of physically interacting self-propelled particles. Despite their simplicity, such models can display complex emergent dynamics, such as motility-induced phase separation (MIPS) [6, 7]. This phenomenon is caused by a self-trapping mechanism whereby particles experience reduced motility at high densities owing to their interactions, eventually leading to dense macroscopic clusters of immotile particles coexisting with a dilute phase of motile particles [6]. Similar phase transitions have been observed in active matter systems with agents that interact through flows [8–12], morphogens [13], social interactions [14], chemotaxis [15], and electrostatic torques [16]. In the past, models for chemically interacting particles have been placed within this framework by representing signals indirectly through a density-dependent motility [6, 17, 18] or an effective physical force [19, 20], but it is not known how far these approaches accurately represent chemical signalling in living matter.

More recently, minimal models of active matter have been supplemented with a concentration field of signalling molecules that mediates the orientation [21–25] or motility [5, 26–28] of cells or particles. Such models have demonstrated that, broadly, repression of motility by intercellular signals tends to promote variations in cell density [5, 27, 29–32], in line with models of physically interacting particles. However, these existing models have limitations. Individual-based or cell-based models are currently too computationally expensive to capture multiscale biological processes over physiologically relevant length and timescales, and existing continuum models often account for gene regulation and chemical signalling using coarse-grained or effective terms, rather than accounting for gene-regulatory kinetics explicitly. Therefore, it is not known in general how the properties of gene-regulatory networks connect to the characteristics of emergent patterns in living active matter.

Here, we develop a multiscale continuum model of chemically interacting particles or cells. Our theory systematically accounts for intracellular processes through careful treatment of the population's gene regulation and phenotype (i.e. motility). Thereby, we connect population-level patterns with the gene-regulatory network inside cells and intercellular QS signalling. We derive a criterion for MIPS mediated by QS in terms of the properties of the gene-regulatory network. We clarify that it is only consistent to approximate chemically mediated interactions by a density-dependent motility in the limit of fast chemical timescales. In general, the density dependence is nonlinear, in contrast to physically interacting active Brownian particles (ABPs) [33–35]. Finally, we identify and explain a new type of MIPS that occurs when cell motility is promoted, rather than repressed, in higher concentrations of QS signal, roughly corresponding to higher cell motility in higher cell densities. This new type of MIPS does not occur in active matter systems in which the interactions are purely physical.

MODEL SETUP

We start by imposing rules at the cell level, before systematically deriving a continuum model from the cell dynamics. We consider a population of N chemically

interacting bacteria, and neglect physical interactions to focus on the role of chemical signalling.

Each cell is denoted by the index i and is located at position $\mathbf{x}_i$ with an internal chemical concentration $u_i(t)$, which represents a gene-regulatory protein or transcription factor. The internal chemical obeys the kinetics

$$\dot{u}_i = f(u_i, c(\mathbf{x}_i, t)) + \sqrt{2\varepsilon}\xi_i(t). \tag{1}$$

Here, f characterises the gene-regulatory network (GRN), and depends on the internal chemical concentration u_i and the local concentration field c of autoinducer (AI), which permeates the population. Although our upscaling is general, we later define f for definiteness. The last term in (1) characterises the stochastic component of the kinetics; ξ_i represents zero-mean Gaussian white noise and ε its magnitude. We work in the limit of small magnitude noise in the gene-regulatory kinetics, $\varepsilon \ll 1$. We include this small noise term for two reasons. Firstly, biochemical reactions are intrinsically stochastic, especially if the reagents are present in small amounts [36]. Secondly, this term regularizes the continuum equations and, as we show below, the system is singular in the limit $\varepsilon \to 0$.

In terms of cell motility, we assume that the cells undergo both active motion and passive diffusion. The active component is characterised by active Brownian motion and run-and-tumble dynamics. Between tumbles, the particle positions $\mathbf{x}_i$ therefore obey

$$\dot{\mathbf{x}}_i = v(u_i)\mathbf{e}_i + \sqrt{2D_t}\boldsymbol{\zeta}_i(t), \tag{2}$$

where $v(u_i)$ is the gene-regulated self-propulsion speed and D_t a translational diffusion coefficient associated with the zero-mean Gaussian white noise $\boldsymbol{\zeta}_i$. The cell orientations are described by the vector $\mathbf{e}_i = (\cos\phi_i, \sin\phi_i)^T$ where the angle ϕ_i undergoes diffusion due to the active Brownian component:

$$\dot{\phi}_i = \sqrt{2D_r(u_i)}\eta_i(t), \tag{3}$$

where D_r is a rotational diffusion coefficient associated with the zero-mean Gaussian white noise η_i.

We derive continuum mean-field equations from the individual-based equations of motion (1)–(3) using standard methods (see Section A of the Supplemental Material [37], c.f. [35, 38, 39]). In the continuum equations, the intracellular chemical concentration u becomes an independent variable for the mean-field variables. That is, the population-level equations are structured in terms of the GRN inside cells; we refer to these multiscale equations as GRN-structured.

The mean-field GRN-structured cell density $n(\mathbf{x}, u, t)$ satisfies

$$\partial_t n = \mathcal{D}(u)\nabla^2 n + \varepsilon\partial_u^2 n - \partial_u\left(f(u,c)n\right), \tag{4a}$$

$$\mathcal{D}(u) := D_t + \frac{v^2(u)}{2\left[\gamma(u) + D_r(u)\right]}. \tag{4b}$$

Here, $\mathcal{D}(u)$ is the effective gene-regulated diffusion coefficient, with γ being the tumble rate. The second term on the RHS of (4a) accounts for the stochastic component of the kinetics. The third term on the RHS of (4a) codifies the GRN through an advection of the mean-field quantities in the u-coordinate. The second term on the RHS of (4b) is the contribution arising from the active Brownian and run-and-tumble dynamics. The physical cell density $\rho(\mathbf{x}, t)$ is related to the GRN-structured cell density n through $\rho = \int_0^\infty n\,\mathrm{d}u$. In deriving equations (4), we consider timescales much longer than the reorientation timescale $(\gamma + D_r)^{-1}$ and lengthscales much larger than the particle persistence length.

Positive feedback is a canonical component of quorum-sensing GRNs, present in many bacterial species [2, 40]. We pose the following specific functional form for f which incorporates positive feedback:

$$f(u, c) = a + \frac{Lc}{K + c} - \lambda u. \tag{5}$$

Here, a represents a constant base production rate of the intracellular chemical u, and λ is a natural decay rate. The second term on the RHS of (5) represents the production of u induced by the local AI concentration c, which constitutes one half of the positive feedback loop illustrated in Figure 1a. This term saturates at a maximal rate of L and has a 'threshold' activation at $c = K$ where the production rate is half-maximal.

The other half of the positive feedback loop in the QS circuit involves the AI concentration field $c(\mathbf{x}, t)$. We assume that AI diffuses passively with coefficient D_c, decays with rate β, and is generated through cell secretion at a rate $\alpha(u)$. Thus, we have

$$\partial_t c = D_c\nabla^2 c - \beta c + \int_0^\infty \alpha(u)n(\mathbf{x}, u, t)\,\mathrm{d}u, \tag{6}$$

where the final term on the RHS is the mean-field secretion term. This term is non-local in u as it encodes the contribution from all internal concentrations in a locally averaged region of space. We emphasize that positive feedback is only present in the QS circuit when the secretion rate $\alpha(u)$ is non-constant across internal concentrations u. For simplicity, we pose a secretion rate that is proportional to the internal concentration, i.e.

$$\alpha(u) = \alpha_0 u. \tag{7}$$

Finally, we assume that the cell population is confined to a rectangular domain Ω, imposing no flux boundary conditions on the boundaries $\partial\Omega$. Hence,

$$\nabla n \cdot \mathbf{N} = 0, \quad \mathbf{x} \in \partial\Omega, \tag{8}$$

where $\mathbf{N}$ is the unit normal on $\partial\Omega$. To ensure physical (i.e. non-negative, bounded) concentrations, we also impose no flux at $u = 0$ and as $u \to \infty$. These conditions correspond to

$$\varepsilon\partial_u n - f(u, c)n = 0, \quad \text{for} \quad u = 0, \quad u \to \infty. \tag{9}$$

Our continuum model therefore consists of the governing equations (4)–(7), and the boundary conditions (8)–(9). The multiscale nature of our model is illustrated schematically in Figure 1a. We verify the predictions of our theory in the following section via numerical simulations of the governing equations, using the open-source finite-element library oomph-lib [41] (see Section E of the Supplemental Material [37]).

INSTABILITY OF THE UNIFORM EQUILIBRIUM STATE

To investigate the emergence of MIPS in our model, we search for instabilities in the *spatially* uniform equilibrium state, emphasizing that this is not *chemically* uniform in general. To this end, we perform a linear stability analysis of the governing equations (4)–(9) to derive an instability criterion for the onset of MIPS.

We derive the steady uniform solution by directly integrating (4a) and imposing the boundary conditions (9). The spatially uniform equilibrium is then given by

$$c_* = \text{const.}, \quad n_e(u) = \rho_* \sqrt{\frac{\lambda}{2\pi\varepsilon}} \exp\left[-\frac{\lambda}{2\varepsilon}(u-u_*)^2\right], \tag{10}$$

where the steady AI concentration c_* and mean internal concentration u_* are defined through the unique positive solution of the algebraic system

$$f(u_*, c_*) = 0, \quad \beta c_* = \alpha_0 \rho_* u_*, \tag{11}$$

where $\rho_* := \int_0^\infty n_e \, \mathrm{d}u$ represents the uniform cell density.

The analysis is singular in the limit $\varepsilon \to 0$, since the equilibrium density n_e (10) formally tends to a Dirac delta function centred at $u = u_*$, representing identical internal concentrations in each cell. To analyse this singular perturbation problem, we perform a WKBJ-like asymptotic approximation and explicitly factor out the singular exponential term. This reduces the analysis to a regular perturbation problem (see Section B of the Supplemental Material [37]).

We perform the linear stability analysis by substituting small perturbations of the form

$$n(\mathbf{x}, u, t) = n_e(u) + \eta(u) e^{i\mathbf{k}\cdot\mathbf{x}+\sigma t}, \quad c(\mathbf{x}, t) = c_* + C e^{i\mathbf{k}\cdot\mathbf{x}+\sigma t}, \tag{12}$$

into the governing equations (4)-(6) and linearizing the result. Here, $\mathbf{k}$ denotes the wavenumber and σ the growth rate of the small perturbations. This yields the dispersion relation (see Section B of the Supplemental Material [37])

$$\sigma + D_c k^2 + \beta - \alpha_0 f_c^* \rho_* \frac{\sigma + (\mathcal{D}_* - \mathcal{D}_*' u_*) k^2}{(\sigma + \mathcal{D}_* k^2)(\sigma + \mathcal{D}_* k^2 + \lambda)} = 0. \tag{13}$$

Here $k := |\mathbf{k}|$ while $\mathcal{D}_* := \mathcal{D}(u_*)$, $\mathcal{D}_*' := \mathcal{D}'(u_*)$, and $f_c^* := \partial_c f(u_*, c_*)$. The spatially uniform steady-state (10) is unstable if Eq. (13) has any root σ with $\mathrm{Re}(\sigma) > 0$. We refer to $\mathcal{D}_*'$ as the motility response since it characterise how the motility responds to changes in internal concentration. We find that there are two types of instability depending on the sign of $\mathcal{D}_*'$.

Case I: Internal chemical represses motility

The first type of instability occurs when higher internal concentrations reduce motility ($\mathcal{D}_*' < 0$), analogous to classic MIPS where higher cell densities reduce motility through physical interaction.

We derive the following instability criterion by substituting $\sigma = 0$ into (13) and rearranging:

$$\frac{\mathcal{D}_*'}{\mathcal{D}_*} < -\frac{A}{u_*}, \tag{14a}$$

where we define

$$A := \frac{1}{\alpha_0 \rho_* f_c^*} \left(\frac{D_c \pi^2}{L_m^2} + \beta\right) \left(\frac{\mathcal{D}_* \pi^2}{L_m^2} + \lambda\right) - 1 > 0. \tag{14b}$$

Here, L_m is the largest side length of the domain, and we use $k = \pi/L_m$ since the longest wavelength mode is always the first to lose stability as $\mathcal{D}_*'$ is decreased from zero (see Section B of Supplemental Material [37]). However, the mode with the largest growth rate, i.e. largest value of $\mathrm{Re}(\sigma)$, typically corresponds to an intermediate wavelength, as shown in Fig 2b.

Eq. (14) is the first key result of our paper. Qualitatively, it states that a spatially uniform population of chemically interacting cells begins to form clusters when the cellular motility (characterized by the diffusion coefficient $\mathcal{D}_*$) is sufficiently repressed in response to perturbations in the internal concentrations. The constant A, defined in (14b), encodes the required strength of repression in terms of the chemical timescales and genetic structure of the population. The mechanism driving the instability is shown schematically in Figure 4a.

The instability criterion (14) reduces to a form reminiscent of the classic instability criterion for physical MIPS (see e.g. equation (3) in [6]) for pure ABPs with no translational diffusion (i.e. $D_r = \text{const.}$, $D_t = \gamma = 0$):

$$\frac{1}{v}\frac{dv}{du}\bigg|_{u_*} < -\frac{A}{2u_*}. \tag{15}$$

Here we use (4b) to express $\mathcal{D}$ in terms of the propulsion speed v. Eq. (15) is the chemical analogue of the well-known instability criterion in active matter without passive diffusion [6]:

$$\frac{1}{V}\frac{dV}{d\rho}\bigg|_{\rho_*} < -\frac{1}{\rho_*}, \tag{16}$$

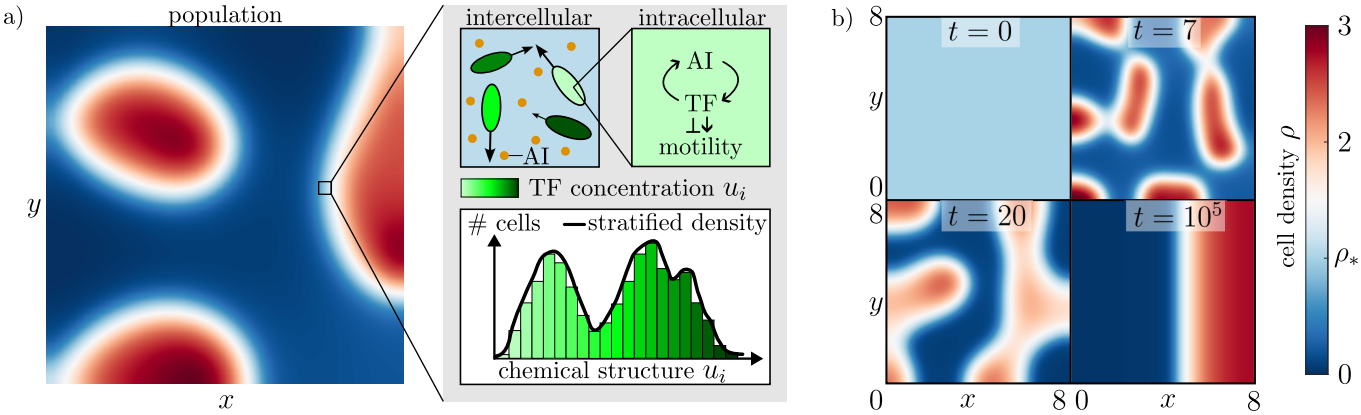

FIG. 1: a) Schematic illustration of our multiscale model of chemically interacting cells. We derive a continuum population model (left), that retains the genetic structure of the population (grey box, right) through chemical stratification. The motility of individual cells depends on their internal chemical concentration. The transcription factor (TF) can either repress or promote motility. The positive feedback mechanism in the gene-regulatory network operates as follows: higher AI concentration increases the production rate of intracellular chemical via the kinetics (5), resulting in locally higher AI concentration through the non-local term in (6). b) Snapshots in time of the cell density from an initially homogeneous state. The AI concentration profile is qualitatively similar to the density profile (see Video S1 in the Supplemental Material [37])

where $V(\rho)$ is the effective density-dependent propulsion speed in classical MIPS. A key difference between (15) and (16) is that the former contains information about the chemical timescales and genetic structure of the population, encoded through the constant A.

If the chemical timescales are very short by comparison to the diffusion time, then u and c are in a quasi-steady state driven by the cell density ρ. In this case u_* can be written in terms of ρ_*, and (15) reduces to (16), but with an additional factor of $1/2$ multiplying the right-hand side. This apparent discrepancy is resolved in Section D of Supplemental Material [37], where we show that to recover (16) the chemical timescales need to be short not just by comparison to the diffusion timescale but also by comparison to the reorientation timescale. In this very-fast-chemical-timescale limit, chemically interacting ABPs are equivalent to physically interacting ABPs. The density-dependent mobility is linear under the additional assumptions of no positive feedback in the QS system, linear kinetics $f(u, c)$, and linear propulsion speed $v(u)$ (see Section D of Supplemental Material [37]). These results suggest that chemical cell-cell interactions can only be approximated as physical interactions under certain conditions.

The dynamics of the cell density ρ are illustrated in Figure 1b, clearly exhibiting MIPS. In Figure 2 we compute the branches of steady-states that bifurcate from the uniform state, and show that the bifurcation point predicted by our analysis in (14a) agrees well with the numerically computed branches. The unstable spatial modes from the dispersion relation $\sigma(k)$, determined

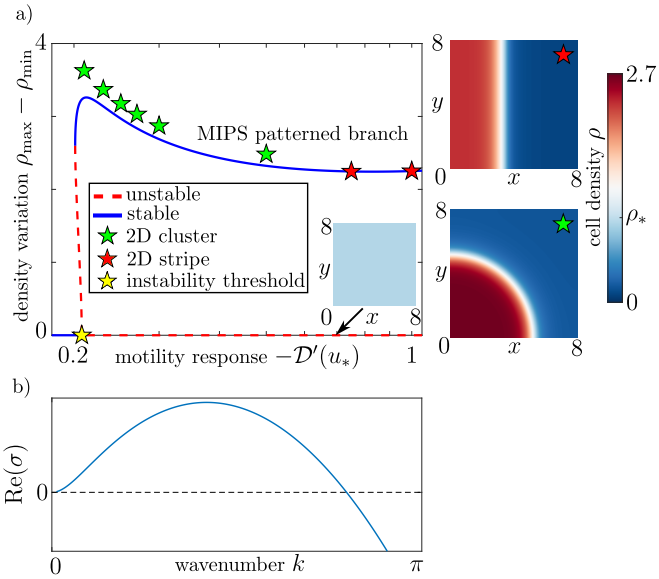

FIG. 2: a) Bifurcation diagram in 1D with 2D steady-state stripe and cluster patterns shown as red and green stars, respectively (see insets and Video S2 in the Supplementary Material). The trivial branch corresponds to (10) and the bifurcating branch is the 1D MIPS-patterned state. The bifurcation point (yellow star) is indistinguishable from that predicted from (14). b) Dispersion relation from linear stability analysis. Parameter values are given in Table 1 of the Supplemental Material [37].

from (13), are illustrated in Figure 2. The spatial mode

with the largest growth rate gives a measure of the size of the clusters that initially form from the uniform state.

Case II: Internal chemical promotes motility

Surprisingly, our linear stability analysis predicts a new type of MIPS instability when higher internal concentrations promote motility ($\mathcal{D}'_* > 0$). Since physical interparticle forces act to reduce motility as density increases, this new instability would not be induced in populations with purely physical interactions. However, chemically interacting populations do not have this restriction; GRNs connected to intercellular signalling can increase cell motility directly in e.g. bacterial swarming where QS regulates flagella assembly [42], and indirectly by e.g. controlling biosurfactant production [3].

Mathematically, this instability occurs when σ is purely imaginary, i.e. via a Hopf bifurcation. The analogue of (14a) for this instability is given by (see Section C of Supplemental Material [37]):

$$\frac{\mathcal{D}'_*}{\mathcal{D}_*} > \frac{B}{u_*}, \tag{17a}$$

where we define

$$B := \frac{\omega_\lambda + \omega}{\omega_0}\left[\frac{(\omega_0+\omega_\lambda)(\omega_0+\omega)}{\alpha_0 f_c^* \rho_*} - 1\right] > 0, \tag{17b}$$

$$\omega_j := \mathcal{D}_* k^2 + j, \quad \omega := D_c k^2 + \beta. \tag{17c}$$

Eq. (17) is the second key result of our paper. It quantifies the condition under which a uniform population of chemically interacting cells undergo spatio-temporal density oscillations. Qualitatively, the population becomes unstable when the cellular motility is sufficiently promoted in response to perturbing the internal concentrations. The constant B, defined in (17b), encodes information about the chemical timescales and genetic structure of the population. In contrast to the instability criterion in (14), the longest wavelength mode, in general, is not the first to become unstable, as can be seen by comparing the dispersion relations for the two instabilities in Figures 2b and 3c. We show the type of spatio-temporal dynamics that arise from this instability in Figure 3a. The oscillations tend to a limit cycle resembling a standing wave pattern, which bifurcates from the uniform state as illustrated by Figure 3b.

The mechanism driving this new oscillatory instability is an effective time delay between local density fluctuations and changes in motility, illustrated schematically in Figure 4b. The time delay is caused by the finite timescales in the QS circuit. To understand this physically, consider a region of locally higher cell density. As the density fluctuation begins to relax, the AI concentration field will increase locally in response to the higher

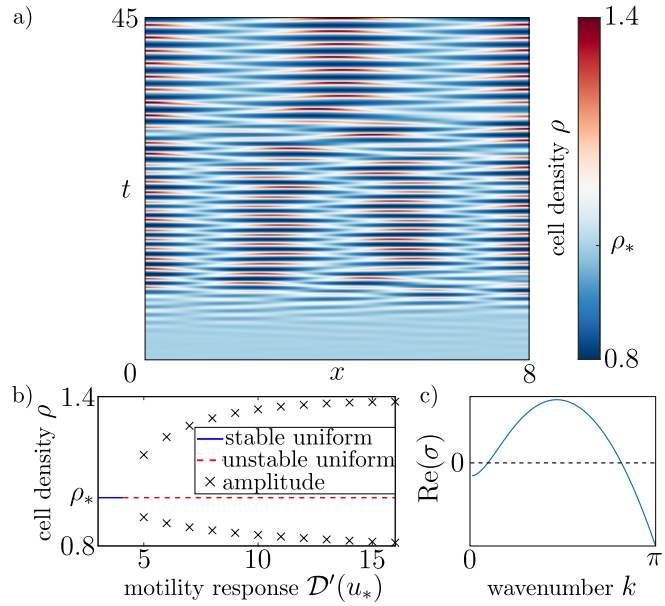

FIG. 3: a) Oscillatory MIPS patterning in 1D showing the formation of periodic spatio-temporal oscillations resembling standing waves (see also Video S3 in the Supplemental Material). b) Bifurcation diagram showing the amplitude of oscillations in the cell density. c) Dispersion relation from the linear theory.

density, which leads to locally higher internal concentrations due to the reaction kinetics. Owing to the chemically regulated swimming speed $\mathcal{D}(u)$, the cells with higher internal concentrations experience a higher motility. As the local density returns to the equilibrium value, the locally higher motility persists and the region begins to deplete of cells, thereby causing the density to 'overshoot' the equilibrium value and form a region of lower density. This forms the first half of the periodic cycle, with the second half having equivalent reasoning. The oscillations will not persist if the effective time delay is too short, because the density will not sufficiently overshoot the equilibrium value when the motility responds too quickly to the relaxing density. The importance of the effective time delay can be seen mathematically by considering the behaviour of B as the delay tends to zero, i.e. in the limit of fast chemical timescales (in which $a \sim L \sim \lambda \sim \alpha_0 \sim \beta$ are large). From (17b), it can be shown that $B \to \infty$ in this limit and hence the criterion (17a) cannot be satisfied, favouring a stable uniform colony.

Our results demonstrate that explicit modelling of gene regulation in cell populations is key to understanding MIPS in living active matter. Our GRN-structured model allows for a direct link between cell-level genetic processes and macroscale pattern formation – in principle, the model can be simplified via a mean-field formulation of the governing equations (4)–(7), but this is only

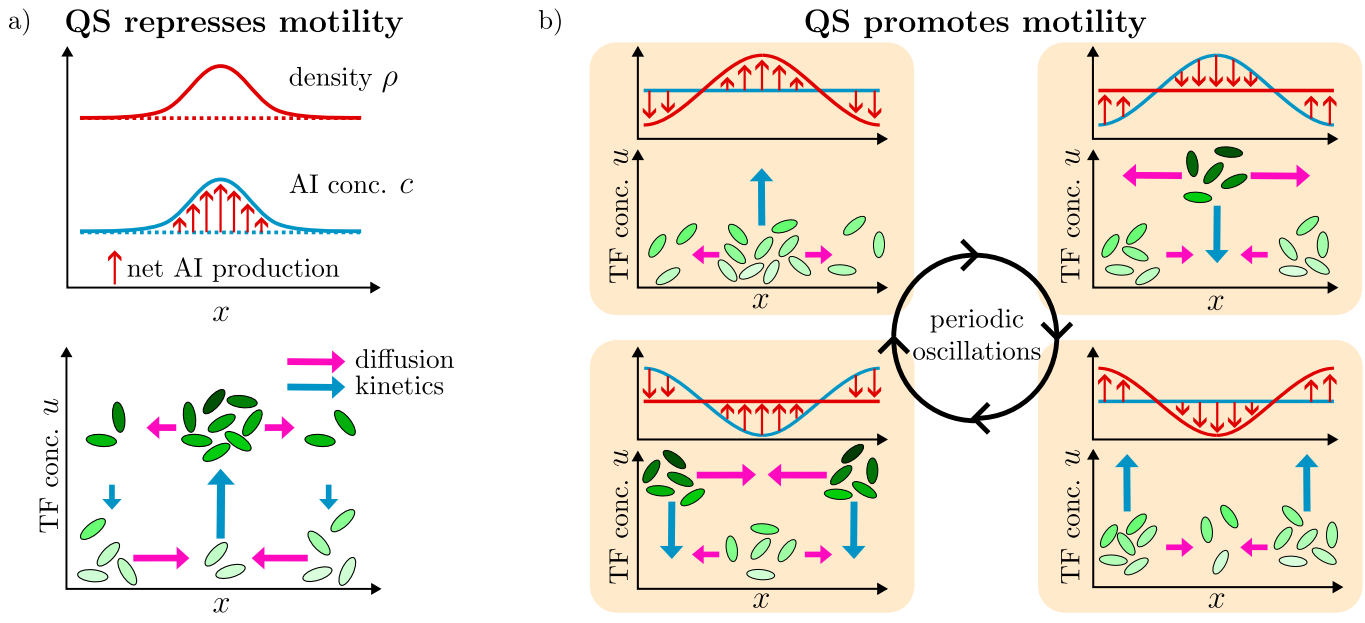

FIG. 4: Schematic illustrations of the instability mechanisms. a) Small density/AI perturbation from the unstable uniform equilibrium in Case I. Pink arrows denote diffusive flux while blue arrows denote chemical flux via the gene-regulatory kinetics. Red arrows correspond to net AI production. In regions of higher AI concentration there is a chemical flux to higher internal concentrations. The density/AI perturbation grows when the motility response $\mathcal{D}'(u)$ is large (and negative) enough for the diffusive flux of high motility cells into the high density region to overcome the diffusive flux of low motility cells out of the high density region. b) Periodic spatio-temporal oscillations in Case II. Owing to finite timescales of gene expression, gradients in AI and internal concentrations persist after density gradients are overcome by motility.

quantitatively accurate near the spatially uniform equilibrium (Supplemental Material [37]). More fundamentally, gene regulation that promotes motility in higher concentrations of chemical signal is required for the oscillatory instability (Hopf bifurcation) that we identify here; this instability would not be present in a system with purely physical interactions between particles. Finally, we note that the linear stability theory for our structured model is extendable to more realistic kinetics, possibly involving multiple internal chemical species or genes.

ACKNOWLEDGEMENTS

The authors thank Devi Prasad Panigrahi and Andrew Hazel for helpful discussions. Furthermore, the authors would like to acknowledge the use of the University of Oxford Advanced Research Computing (ARC) facility in carrying out this work, http://dx.doi.org/10.5281/zenodo.22558, as well as the UCL Mathematics Department for use of the high performance cluster. W. J. M. R. is grateful for financial support in part from an NSERC PGSD scholarship and in part from Somerville College. M. P. D. is supported by the UK Engineering and Physical Sciences Research Council [EP/W032317/1]. P. P. is supported by a UKRI Future Leaders Fellowship [MR/V022385/1].

* wesley.ridgway@some.ox.ac.uk
† m.dalwadi@ucl.ac.uk
‡ philip.pearce@ucl.ac.uk
§ chapman@maths.ox.ac.uk

[1] A. Deutsch, P. Friedl, L. Preziosi, and G. Theraulaz, "Multi-scale analysis and modelling of collective migration in biological systems," *Philosophical Transactions of the Royal Society B*, vol. 375, no. 1807, p. 20190377, 2020.

[2] K. Papenfort and B. L. Bassler, "Quorum sensing signal–response systems in Gram-negative bacteria," *Nature Reviews Microbiology*, vol. 14, no. 9, pp. 576–588, 2016.

[3] R. Daniels, J. Vanderleyden, and J. Michiels, "Quorum sensing and swarming migration in bacteria," *FEMS Microbiology Reviews*, vol. 28, no. 3, pp. 261–289, 2004.

[4] L. E. Weiss, J. P. Badalamenti, L. J. Weaver, A. R. Tascone, P. S. Weiss, T. L. Richard, and P. C. Cirino, "Engineering motility as a phenotypic response to LuxI/R-dependent quorum sensing in *Escherichia coli*," *Biotechnology and Bioengineering*, vol. 100, pp. 1251–1255, 8 2008.

[5] C. Liu *et al.*, "Sequential establishment of stripe patterns in an expanding cell population," *Science*, vol. 334, pp. 238–241.

[6] M. E. Cates and J. Tailleur, "Motility-Induced Phase Separation," *Annual Review of Condensed Matter Physics*, vol. 6, no. 1, pp. 219–244, 2015.

[7] B. Partridge and C. F. Lee, "Critical Motility-Induced Phase Separation Belongs to the Ising Universality Class," *Physical Review Letters*, vol. 123, no. 6, p. 068002, 2019.

[8] R. A. Simha and S. Ramaswamy, "Hydrodynamic Fluctuations and Instabilities in Ordered Suspensions of Self-Propelled Particles," *Physical Review Letters*, vol. 89, p. 058101, 2002.

[9] S. Ramaswamy, "The Mechanics and Statistics of Active Matter," *Annual Review of Condensed Matter Physics*, vol. 1, pp. 323–345, 2010.

[10] S. Bhattacharyya and J. M. Yeomans, "Phase Separation Driven by Active Flows," *arXiv preprint arXiv:2302.00153*, 2023.

[11] T. H. Tan, A. Mietke, J. Li, Y. Chen, H. Higinbotham, P. J. Foster, S. Gokhale, J. Dunkel, and N. Fakhri, "Odd dynamics of living chiral crystals," *Nature*, vol. 607, no. 7918, pp. 287–293, 2022.

[12] I. Aranson, "Bacterial active matter," *Reports on Progress in Physics*, vol. 85, p. 076601, 2022.

[13] S. Bhattacharyya and J. M. Yeomans, "Coupling Turing stripes to active flows," *Soft Matter*, vol. 17, no. 47, pp. 10716–10722, 2021.

[14] C. Anderson and A. Fernandez-Nieves, "Social interactions lead to motility-induced phase separation in fire ants," *Nature Communications*, vol. 13, no. 1, p. 6710, 2022.

[15] G. Courcoubetis, M. S. Gangan, S. Lim, X. Guo, S. Haas, and J. Q. Boedicker, "Formation, collective motion, and merging of macroscopic bacterial aggregates," *PLoS Computational Biology*, vol. 18, no. 1, p. e1009153, 2022.

[16] J. Zhang, R. Alert, J. Yan, N. S. Wingreen, and S. Granick, "Active phase separation by turning towards regions of higher density," *Nature Physics*, vol. 17, no. 8, pp. 961–967, 2021.

[17] X. Yang, D. Marenduzzo, and M. C. Marchetti, "Spiral and never-settling patterns in active systems," *Physical Review E*, vol. 89, p. 012711, 2014.

[18] T. Grafke, M. E. Cates, and E. Vanden-Eijnden, "Spatiotemporal Self-Organization of Fluctuating Bacterial Colonies," *Physical Review Letters*, vol. 119, p. 188003, 2017.

[19] C. Abaurrea Velasco, M. Abkenar, G. Gompper, and T. Auth, "Collective behavior of self-propelled rods with quorum sensing," *Physical Review E*, vol. 98, p. 022605, 2018.

[20] F. Jose, S. K. Anand, and S. P. Singh, "Phase separation of an active colloidal suspension *via* quorum-sensing," *Soft Matter*, vol. 17, no. 11, pp. 3153–3161, 2021.

[21] A. Ziepke, I. Maryshev, I. S. Aranson, and E. Frey, "Multi-scale organization in communicating active matter," *Nature Communications*, vol. 13, no. 1, p. 6727, 2022.

[22] H. Zhao, A. Košmrlj, and S. S. Datta, "Chemotactic motility-induced phase separation," *arXiv preprint arXiv:2301.12345*, 2023.

[23] F. R. Macfarlane, T. Lorenzi, and K. J. Painter, "The Impact of Phenotypic Heterogeneity on Chemotactic Self-Organisation," *Bulletin of Mathematical Biology*, vol. 84, no. 12, p. 143, 2022.

[24] R. Erban and H. G. Othmer, "From Individual to Collective Behavior in Bacterial Chemotaxis," *SIAM Journal on Applied Mathematics*, vol. 65, no. 2, pp. 361–391, 2004.

[25] S. Yasuda, "Effects of internal dynamics on chemotactic aggregation of bacteria," *Physical Biology*, vol. 18, p. 066001, 2021.

[26] X. Fu, L.-H. Tang, C. Liu, J.-D. Huang, T. Hwa, and P. Lenz, "Stripe Formation in Bacterial Systems with Density-Suppressed Motility," *Physical Review Letters*, vol. 108, p. 198102, 2012.

[27] X. Xue, C. Xue, and M. Tang, "The role of intracellular signaling in the stripe formation in engineered *Escherichia coli* populations," *PLOS Computational Biology*, vol. 14, p. e1006178, 6 2018.

[28] X. Zhang and N. Mitarai, "Finite response time in stripe formation by bacteria with density-suppressed motility," *arXiv preprint arXiv:1905.02933*, 2019.

[29] M. Rein, N. Heinß, F. Schmid, and T. Speck, "Collective Behavior of Quorum-Sensing Run-and-Tumble Particles under Confinement," *Physical Review Letters*, vol. 116, p. 058102, 2016.

[30] J. Smith-Roberge, D. Iron, and T. Kolokolnikov, "Pattern formation in bacterial colonies with density-dependent diffusion," *European Journal of Applied Mathematics*, vol. 30, pp. 196–218, 2 2019.

[31] A. Fischer, F. Schmid, and T. Speck, "Quorum-sensing active particles with discontinuous motility," *Physical Review E*, vol. 101, p. 012601, 2020.

[32] T. Bäuerle, A. Fischer, T. Speck, and C. Bechinger, "Self-organization of active particles by quorum sensing rules," *Nature Communications*, vol. 9, p. 3232, 12 2018.

[33] Y. Fily and M. C. Marchetti, "Athermal Phase Separation of Self-Propelled Particles with No Alignment," *Physical Review Letters*, vol. 108, p. 235702, 2012.

[34] J. Stenhammar, A. Tiribocchi, R. J. Allen, D. Marenduzzo, and M. E. Cates, "Continuum Theory of Phase Separation Kinetics for Active Brownian Particles," *Physical Review Letters*, vol. 111, p. 145702, 2013.

[35] J. Bialké, H. Löwen, and T. Speck, "Microscopic theory for the phase separation of self-propelled repulsive disks," *Europhysics Letters*, vol. 103, no. 3, p. 30008, 2013.

[36] D. T. Gillespie, A. Hellander, and L. R. Petzold, "Perspective: Stochastic algorithms for chemical kinetics," *The Journal of Chemical Physics*, vol. 138, no. 17, p. 170901, 2013.

[37] See Supplemental Material for details regarding the derivation of the governing equations, analysis of the linear stability problem, the Hopf bifurcation criterion, reduction to classical MIPS, numerical methods, and comparison with a mean-field model.

[38] J. Bialké, T. Speck, and H. Löwen, "Active colloidal suspensions: Clustering and phase behavior," *Journal of Non-Crystalline Solids*, vol. 407, pp. 367–375, 2015.

[39] M. E. Cates and J. Tailleur, "When are active Brownian particles and run-and-tumble particles equivalent? Consequences for motility-induced phase separation," *Europhysics Letters*, vol. 101, no. 2, p. 20010, 2013.

[40] M. P. Dalwadi and P. Pearce, "Emergent robustness of bacterial quorum sensing in fluid flow," *Proceedings of the National Academy of Sciences*, vol. 118, no. 10, p. e2022312118, 2021.

[41] M. Heil and A. L. Hazel, "oomph-lib–an *O*bject-*O*riented *M*ulti-*P*hysics Finite-Element *L*ibrary," in *Bungartz, HJ., Schäfer, M. (eds) Fluid-Structure Interaction*, vol. 53, pp. 19–49, Springer (Lecture Notes on Computational Science and Engineering), 2006.

[42] V. Sperandio, A. G. Torres, and J. B. Kaper, "Quorum sensing *Escherichia coli* regulators B and C (QseBC): a novel two-component regulatory system involved in the regulation of flagella and motility by quorum sensing in *E. coli*," *Molecular Microbiology*, vol. 43, no. 3, pp. 809–821, 2002.